A COMPARATIVE LOOK AT ATOMIC OXYGEN AND CARBON DIOXIDE NEUTRAL DENSITIES ON MARS USING DATA FROM THE MAVEN SATELLITE MISSION

by

EMILY ANN CURTIS

Presented to the Faculty of the Graduate School of

The University of Texas at Arlington in Partial Fulfillment

of the Requirements

for the Degree of

MASTER OF SCIENCE IN PHYSICS

THE UNIVERSITY OF TEXAS AT ARLINGTON

August 2020

ACKNOWLEDGEMENTS

I would like to express my sincere gratitude to my Supervising Professor, Dr. Yue Deng, for her supportive guidance not only throughout the research process, but also in helping me navigate graduate school. This journey would not have been possible without her support, and I am truly grateful for the opportunity she provided me.

I would also like to thank all the members of my Supervising Committee: Dr. Yue Deng, Dr. Yingjuan Ma and Dr. Sangwook Park. I greatly appreciate the time and expertise that you devoted to this project and am extremely fortunate that you agreed to be on my committee.

April 21, 2020

ABSTRACT

A COMPARATIVE LOOK AT ATOMIC OXYGEN AND CARBON DIOXIDE NEUTRAL DENSITIES ON MARS USING DATA FROM THE MAVEN SATELLITE MISSION

Emily Ann Curtis, MS

The University of Texas at Arlington, 2020

Supervising Professor: Yue Deng

This thesis uses the level 2 limb scan data from the IUVS instrument onboard the MAVEN satellite to investigate the density distributions of O and CO_2 in the lower thermosphere of Mars. In addition to examining the density as a function of spatial position, the dependencies on SZA and local time are also inspected. The data used in the study are during the time interval between October 2014 and June 2018.

Results of this study show that the density of CO_2, the major species on Mars, is predominantly driven by typical atmospheric forces related to solar irradiation absorption. An atmosphere wave 2 structure

appears clearly when examining the average density variation over longitudes, and an inverse relationship between the solar zenith angle and density occurs above 50 degrees SZA. During the spring and autumn equinox, the density distribution peaks about the equatorial region, and the dependence on local time shows that the density peaks in the afternoon. However, the same studies with the O data show more variations at all altitudes, which lead to the conclusion that O is being strongly affected by other driving forces even in the thermosphere as low as 120 km. The study of CO_2 and O will contribute to primary knowledge of the Martian thermosphere and improve understanding of the driving forces that affect these species.

TABLE OF CONTENTS

LIST OF FIGURES

LIST OF TABLES

Table Page

CHAPTER 1

INTRODUCTION TO MARS

1.1 Why Mars?

Mars is the fourth planet from the Sun and has been a component of human history for millennia due to its visibility in the night sky even without the need for a telescope (Figure 1.1). From as early as the 1500's, observations of Mars have led to discovering many physical properties about our solar system and planetary motion; not the least of which being Kepler's first law, which states that orbits are inherently elliptical rather than circular [13]. With the improvement in technologies and capability of space exploration developed during the 20th century, Mars has remained a point of interest to scientists today. The further study of Mars hopes to answer questions regarding the history of the solar system, such as what happens to planets over time and why is there variation between planets in this process, and can there be life outside of Earth [13]. There is still a broad scope of subjects to learn about, and because of this there is a continual need for an array of studies to be done about Mars. In this thesis, the focus will be on the climatological description of variation of

different constituents in the upper atmosphere of Mars, which will strongly help discover the driving physical processes.

Figure 1.1. An illustration of Mars (Courtesy of NASA/JPL-Caltech).

1.2 Properties of the Atmosphere

A planetary atmosphere is comprised of layers of gas and plasma gathered around that planet by the gravitational force. These layers are generally defined by their components and properties and are common across differing bodies, although the significant processes that happen in these layers are unique to the chemical composition of the atmosphere and depend on other properties of the planet such as the presence of a magnetic field. The layers can be split into two major groupings: the lower atmosphere, which is well-mixed with a constant scale height across

different neutral species, and the upper atmosphere. Both layers can be further defined, but since this study will focus on the upper atmosphere, we will only discuss it in further detail. The thermosphere, ionosphere, and exosphere all contribute to the upper atmosphere system. The exosphere is the topmost region of the atmosphere that borders space; there are gas particles in the exosphere, but the number density is so small that it is essentially a collision-less region [18]. The ionosphere overlaps the exosphere and thermosphere, but it is the region composed of charged particles; the movement of these particles causes the ionosphere to act as a conducting sheet [18]. The thermosphere is an important region because it connects the neutral lower atmosphere to the exosphere and contributes to the dynamics between these regions [16]. Meanwhile, the thermosphere and ionosphere are strongly coupled into each other through ion-neutral collisions. Figure 1.2 illustrates the altitude boundaries of these layers on Mars. These boundaries are influenced by seasonal variation and solar irradiation, so they are not static by any means. For comparison, the thermosphere on Earth is from about 90 to 500 km, the exosphere extends beyond that, and the ionosphere ranges from about 60 to 1000 km [18].

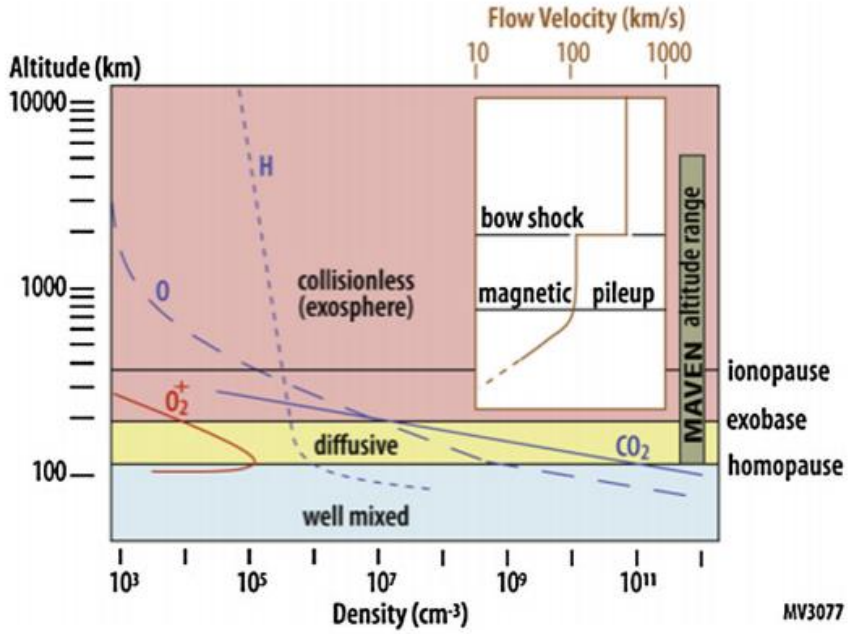

Figure 1.2. Description of the atmospheric layers on Mars. The thermosphere extends from the homopause to the exobase (from [8]).

With an orbiting, rotating planet, it is also necessary to define some other concepts relating to the geometry of the planet. The local time (LT) is described with respect to the Sun's position over a given coordinate location at the surface of the planet: for Earth, the time ranges from 0 to 24 and noon, or 12, is the time at which the Sun is at its highest point over that location. The length of a day on Mars is just 40 minutes longer than that on Earth [18]. The solar zenith angle (SZA) measures the angle between the zenith at a location and the center of the Sun's disc, where the subsolar point occurs at 0^0 latitude, and the dayside is in any measurement less than 90 degrees. Earth is unique in that it has an

almost circular orbit, but in fact elliptical orbits are the norm, and Mars has an elliptical orbit with an eccentricity of 0.0934 and a period of approximately 1.88 Earth years [2]. A comparison of the orbits of Earth and Mars is shown in Figure 1.3. The solar longitude (Ls) describes the position of a planet in its orbit about the Sun. For Mars, the northern hemisphere summer solstice occurs at 90^0 Ls, the northern hemisphere winter solstice occurs at 270^0 Ls (Figure 1.4), and the closest approach to the Sun is at 250^0 Ls [14].

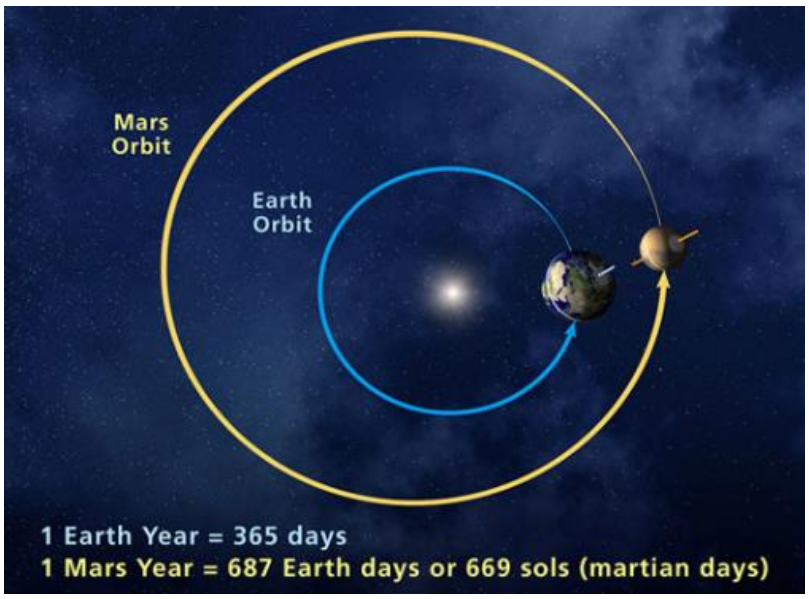

Figure 1.3. Cartoon showing the approximate orbits of Earth and Mars. Mars takes almost twice as long to orbit the Sun (Courtesy of NASA/JPL-Caltech).

Thermodynamics indicates that if heat is added to a system, the system will expand and become dynamic in response. The heat or energy inputs into an atmospheric system include the solar extreme ultraviolet (EUV) rays from 10 to 120 nm, and solar wind which interacts with the ionosphere and in turn influences the processes in the thermosphere [7]. Exposure to solar EUV is maximized at the subsolar point and the noon local time, which depend on the seasonal geometry of the planet's orbit and axis tilt, and the solar activity level. The major species in the atmosphere are likely to respond to changes in these variables as the atmosphere as a whole acts according to the laws of thermodynamics. These effects are well-described on Earth due to the numerous studies that have been done, but less examined for conditions on Mars due to the limited availability of information.

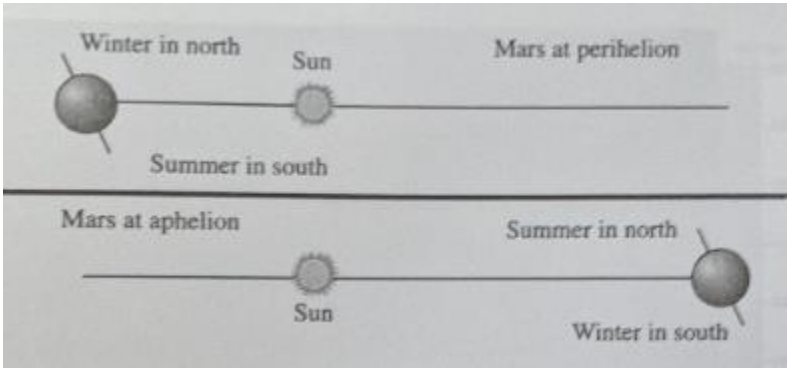

Figure 1.4. A perpendicular view of the Martian orbit. Northern hemisphere winter occurs when Mars is closest to the Sun, and northern hemisphere summer occurs when Mars is further away in the elliptical orbit (from [18]).

It has been long speculated that the climate on Mars has changed over time (Figure 1.5). Evidence in the geologic records shows patterns of erosion that would be caused from liquid running over a surface for long periods of time [3]; however, current conditions on Mars make liquid water unstable at the surface [9]. These features are present on surfaces that are at least 3.7 billion years old, so it is believed that greenhouse gases were present in the Martian atmosphere to create higher temperature and pressure conditions to sustain water but have since been lost [8]. The Viking program that launched in 1975 was the first mission to successfully land on Mars. There were two Viking landers that took in situ data upon entry to the Martian atmosphere [17]. Prior to 2014, data from the Martian atmosphere in the region below 200 km were limited to these two single measurements and data collected from the Curiosity rover at the surface as part of the Mars Science Laboratory mission that landed on Mars in 2012 [11]. By that time, there were several missions around Mars capable of collecting upper atmosphere data. In fact, the Mars Express spacecraft recorded ions in the process of being stripped away by the solar wind [1]. This further solidified the idea of significant atmospheric loss on Mars, but there were no missions that exclusively focused on these processes.

Figure 1.5. An artist's depiction of the view of the surface of Mars about 4 billion years ago (left) compared to how Mars currently looks (right) (Courtesy of NASA).

1.3 MAVEN Mission

A more comprehensive exploration into the Martian atmosphere was required in order to continue studying the processes unique to Mars. Thus, NASA launched the Mars Atmosphere and Volatile Evolution (MAVEN) mission in late 2013. MAVEN began orbiting Mars in 2014, and immediately started collecting data to meet its three science objectives: 1) to measure the composition and structure of the upper atmosphere today and determine the controlling processes of the atmosphere, 2) to measure

the rate of atmospheric loss ongoing today and determine the controlling processes, 3) use the information gathered about ongoing processes to extrapolate back in time and determine the total amount of atmospheric loss over Mars' 4.5 billion year history [8]. MAVEN was the first mission to Mars solely dedicated to studying the upper atmosphere (Figure 1.6).

Figure 1.6. An artist's rendering of MAVEN orbiting Mars (Courtesy of NASA).

MAVEN has eight science instruments onboard to take a range of in situ and remote measurements. It establishes ion and neutral density composition at a range of altitudes via the Imaging Ultraviolet Spectrograph (IUVS) and Neutral Gas and Ion Mass Spectrometer

(NGIMS), and also measures variables such as magnetic fields, solar wind, and solar EUV to create a meticulous picture of energy input and flow through the atmospheric system. The satellite follows an elliptical orbit to gather data over all regions of Mars, although global coverage at a single moment is not possible. The orbit MAVEN follows is shown in Figure 1.7. Apoapsis occurs at a fixed altitude, while periapsis is determined to occur when the atmospheric density is between 0.05–0.15 kg/km^3 [8].

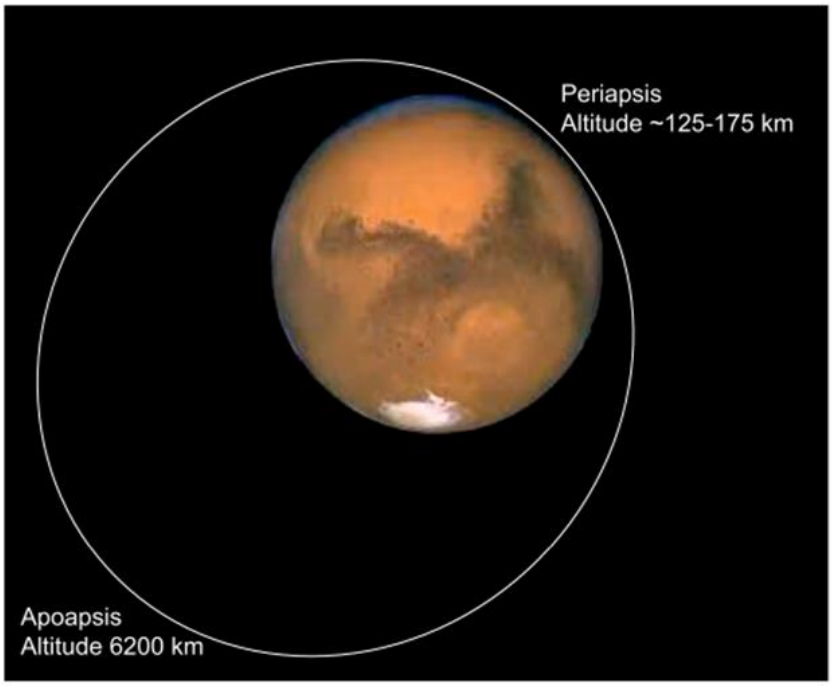

Figure 1.7. An illustration of the MAVEN orbit to scale with Mars (from [8]).

1.4 Thesis Objective

The data from MAVEN have contributed to a variety of studies, from describing the seasonal dust storms that Mars experiences to modelling the photochemical and ion escape rates. The primary focus of this thesis is to complete a systematical data analysis on the direct results from the MAVEN IUVS measurements in order to determine the climatological variations that currently occur among two major neutral species in the Martian thermosphere, oxygen and carbon dioxide.

Here, the motivation to explore Mars and a general description of the Martian atmosphere have been discussed. Chapter 2 details the methodology employed to study the variation of neutral oxygen and carbon dioxide with respect to location and planetary geometry, and Chapter 3 discusses the results discovered from this study. Chapter 4 offers some final conclusions as well as possible directions of future works.

CHAPTER 2

METHODOLOGY

2.1. Purpose

The MAVEN mission has been collecting data to reveal atmospheric properties and processes since reaching Mars and beginning its primary mission phase in 2014 [8]. Onboard MAVEN, the IUVS is a complex instrument that uses 115 to 330 nm ultraviolet emissions to create spatial maps and vertical profiles of neutral and ion densities across a wide range of altitudes, from the lower atmosphere to thousands of kilometers above the surface [15].

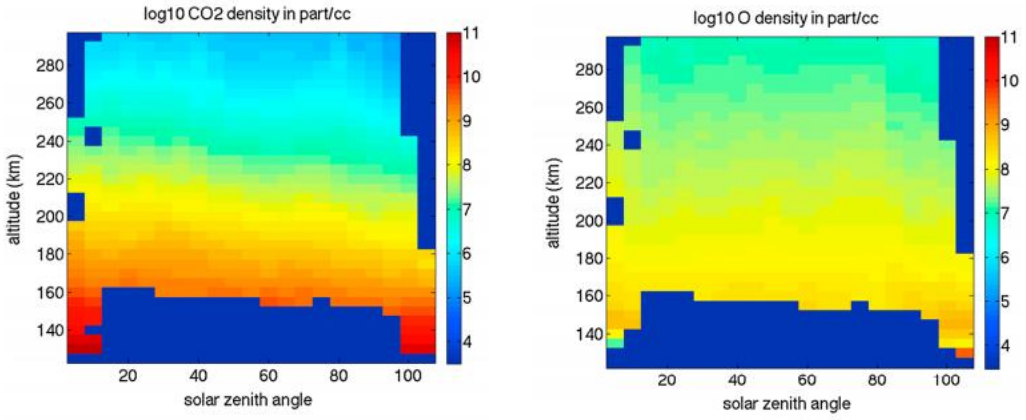

Figure 2.1. CO_2 density (left) and O density (right) as measured by MAVEN NGIMS. Densities are plotting using a log scale, and areas with missing data are shown in dark blue (from [12]).

This study utilizes the IUVS data to investigate the density distributions of two neutral species, atomic oxygen and carbon dioxide, throughout the thermosphere, and under the consideration of spatial location, solar zenith angle and local time. Carbon dioxide was chosen due to its being the major constituent in this region of the thermosphere [17], and atomic oxygen was selected due to the importance of the species in defining hot oxygen escape rates, which is believed to be the major source of neutral atmospheric loss today. Hot oxygen production is dependent on O_2^+ ions, and collisions that affect loss primarily occur between O and CO_2 [10]. The study of these two species aims to contribute to primary knowledge of the thermosphere and improve understanding of the driving forces that affect these species.

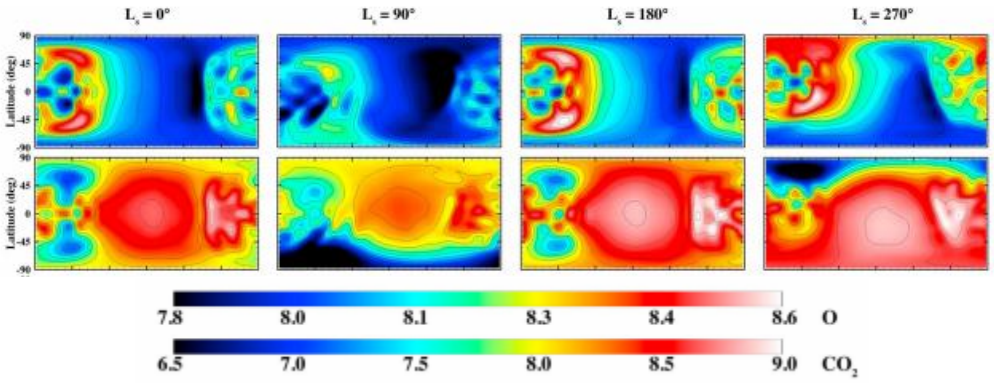

Figure 2.2. M-GITM simulation results of O (top) and CO_2 (bottom) at 200 km for the four seasonal conditions. Densities are measured as cm^{-3} in the log scale (from [10]).

There have been other studies published regarding the density of these species. In 2015, Mahaffy et al. examined the neutral density data from the Neutral Gas and Ion Mass Spectrometer (NGIMS) onboard MAVEN. Figure 2.1 illustrates the variation of CO_2 and O density as a function of altitude and SZA in the Northern winter period. Across a set altitude, CO_2 density decreases with increasing SZA, and O density does not drop off as quickly as CO_2 above 200 km [12]. Several studies have also showed model results of thermospheric variations. Lee et al. [2015] revealed the distributions of background neutral species from the Mars Global Ionosphere Thermosphere Model (M-GITM) simulations, which have been used in calculations of hot oxygen escape. In Figure 2.2, the simulated seasonal O and CO_2 densities at approximately 200 km are presented under solar minimum conditions. The oxygen distribution is inversely correlated to that of carbon dioxide [10].

These next figures were developed using coronal scan data from the MAVEN IUVS. Chaufray et al. [2015] compiled IUVS radiance spectra from the Far Ultraviolet (FUV) detector during the outbound phase of a single orbit (Figure 2.3). The signal for O I is emitted at 130.4 nm, and while the signal gets weaker as the altitude increases, between 100 and 250 km, the oxygen emission is measurable with a spatial resolution of about 5 km [5]. The other emission clearly visible at all altitudes is the

121.6 nm Hydrogen line. Mars is known to have a Hydrogen corona that extends far into the exosphere [4], and the Lyman-alpha emission makes the H corona observable. While not visible here, CO_2 density can be determined through a combination of several different carbon signals; most of which are found between 180 and 330 nm, which is measured by the middle ultraviolet (MUV) detector [15].

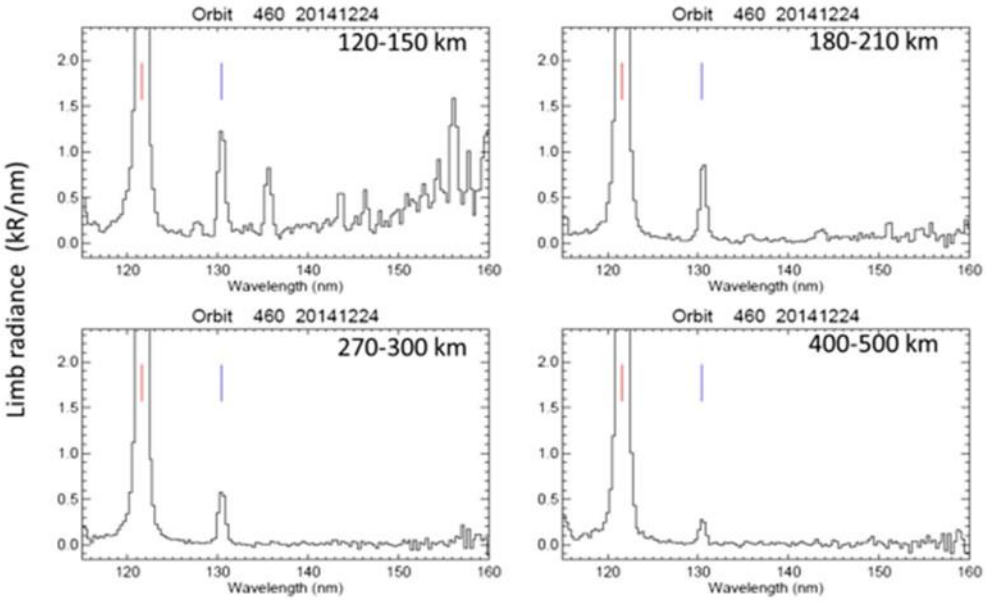

Figure 2.3. IUVS spectra of O I 130.4 nm resonance and H Lyman-alpha emissions. These spectra were measured by the FUV detector, which detects emissions between 115 and 180 nm (from [5]).

There are two distinct oxygen populations present in the Martian atmosphere: hot oxygen and cold oxygen. They are both neutral atomic O species, but the difference comes from how they are formed. Hot oxygen is the product of the dissociative recombination reaction of O_2^+. This is an

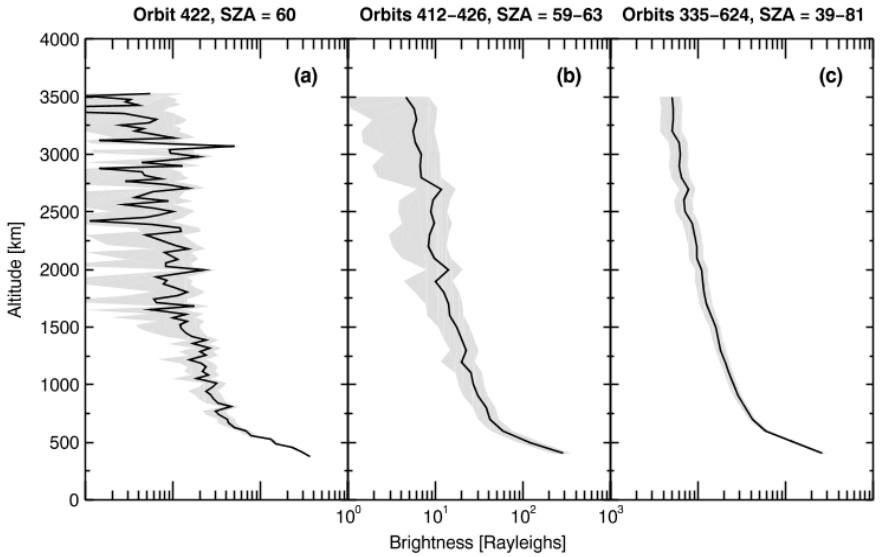

Figure 2.4. Vertical profiles of O from IUVS coronal scans. Data from 1 orbit (left), 5 orbits (middle), and 48 orbits (right) show that as the sample size is increased, the wave structure and uncertainties are smoothed (from [6]).

exothermic reaction, so the neutral oxygen produced from this reaction gains energy. If the oxygen atoms have enough energy, this can lead to photochemical escape, otherwise the hot O will be trapped by the gravitational force and form the hot O corona. The cold O is the non-energetic, neutral background species, and so it is predominant through the thermosphere. Figure 2.4 shows vertical profiles of oxygen assimilated by Deighan et al. [2015] using IUVS coronal scans. The two O populations are discernable by having different scale heights [10]. From this data, the boundary at which the hot oxygen becomes more prevalent than cold

oxygen in the atmosphere is 600 km. Even with the work that has been done thus far, there are still gaps in our knowledge of the thermosphere climatology from analyzing the data products, which is the focus of this research.

2.2. Methods

MAVEN has eight science instruments onboard to make a range of observations; for this paper, data from the MAVEN IUVS is exclusively presented. The IUVS has four different modes of operation to make quantitative measurements, and all the modes utilize UV emissions to collect data about the atmosphere. The four modes are as follows: disk mapping, coronal scans, stellar occultations, and limb scans. Disk mapping creates two-dimensional images of neutral species and dust over the planetary disk. Coronal scans are used to measure the densities of hot species (H, O, and N) above 200 km. Stellar occultations probe the Martian mesosphere and lower thermosphere for ozone and carbon dioxide, but the instrument orientation must be properly aligned with a star. Limb scans create vertical profiles of several neutral species and ions between 100 km to 225 km. Each mode requires a unique orientation, so different modes operate as MAVEN goes through its elliptical orbit [15]. The limb scans, which sourced the data used here, are taken during the

periapsis phase of MAVEN's orbit and the geometry is shown in Figure 2.5.

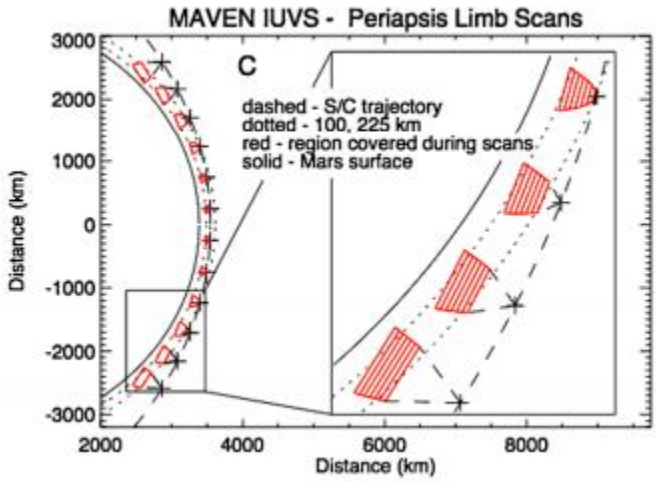

Figure 2.5. An illustration of the geometry of limb scan measurements taken during spacecraft periapsis. For each orbit, 12 limb scans are taken, and each limb scan covers the altitude range between 100 and 225 km (from [15]).

In this study, the density of neutral oxygen and carbon dioxide was investigated using the available level 2 limb scan data from October 2014 through June 2018. The data are available from the public data source at the University of Colorado Boulder Laboratory for Atmospheric and Space Physics (LASP) MAVEN Science Data Center (https://lasp.colorado.edu/maven/sdc/public/data/sci/). The data coverage in terms of time is shown in Table 2.1 and clearly the existing level 2 data set for the four-year time frame is not complete, and in fact there are fourteen months during this time interval with no data available.

Table 2.1. The months without level 2 data available at the time of writing.

Months	December	January February June July December	January February July August September	February August	February
Year	2014	2015	2016	2017	2018

Atomic oxygen was initially chosen for this study due to the significance of hot oxygen escape under current conditions on Mars, and carbon dioxide data were collected to use as a reference due to it being the major species on Mars. In each limb scan, there were three altitudes with density data recorded; these altitudes were approximately around 120 km, 140 km and 170 km. The altitude data were binned in ranges to not exclude any outlier data. The figures labelled as being at “120 km” were collected using data between 100 and 130 km, the figures labelled at “140 km” were assembled from data between 130 and 150 km, and the figures showing data at “170 km” were compiled from the altitudes ranging from 150 to 180 km.

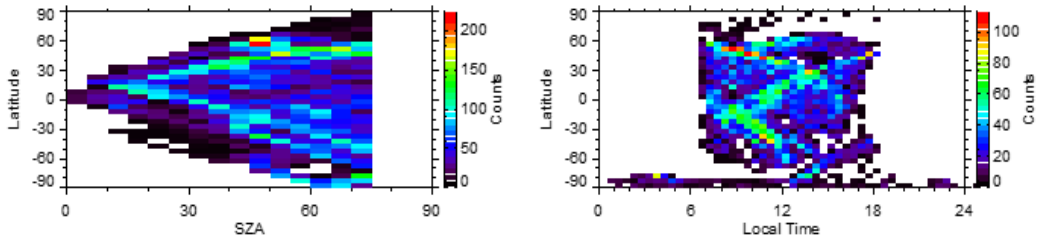

Figure 2.6. Data coverage as a function of latitude and SZA (left) and latitude and LT (right). Number counts show the number of orbits that collected data that falls within each bin, not the total data.

For each altitude, two figures were created for each species. The first figures are density maps, which plot out the average density of O and CO_2 in each bin as a function of latitude, longitude, solar zenith angle (SZA), or local time (LT). The unit for all densities shown in this paper is number of particles per cubic centimeter. Latitude is binned in 5-degree increments, while the longitude is binned in 15-degree increments, the SZA is binned in 5-degree increments, and the local time is binned in 30-minute (half-hour) increments. Before plotting the average density in these bins, data coverage maps for each of these variables were created as a proof of concept to show if there were enough data available to generate statistically meaningful results for this study. Figure 2.6 shows the number of orbits that have data points in each bin when we bin the data according to the LT and SZA. Since there are twelve limb scans done every orbit, the actual number of data points for each species is up to twelve times what is shown. Inside each bin, an average density is calculated and shown in

Chapter 3 only when there are greater than or equal to 5 data points in that bin. The LT and SZA figures were then created using all the data from October 2014 thru June 2018 due to fact that limited amount of data are available in some of the bins split by further conditions, such as season. However, for the latitude versus longitude maps, the data coverage was more uniform, with each bin containing on average more measurements. When split by species and altitude, each bin still had several hundred data points. Since MAVEN does not have global coverage at one time, it was then decided that further separating the data by Martian seasons would produce more meaningful results when looking at the dependency on latitude and longitude. To do this, all data from the Northern hemisphere summer (Ls= 60^0, 150^0) and winter (Ls= 240^0, 330^0) were excluded, leaving only the data from the spring and autumn equinox, which kept more than 50% of the total data in the latitude range we were interested in for further analysis (Figure 2.7).

The second set of figures created for each species are line graphs which further average the density over either latitude, longitude, SZA or LT to study the dependence of density on that variable. For the latitude and longitude line plots, only data that falls between latitudes of -60^0 to 60^0 is averaged. Due to the variation of data coverage, the latitudinal range is revised to -30^0 to 30^0, and -15^0 to 15^0 for the LT line plots and SZA line

graphs respectively. Even though the summer and winter outlier data are included for the LT and SZA figures, most of the extreme data from those seasons lies outside of these latitude ranges, so seasonal changes should not strongly influence the average densities calculated in each bin. Density averages in the line plots were created by calculating the means of density across the bins of the variable being averaged in the density maps.

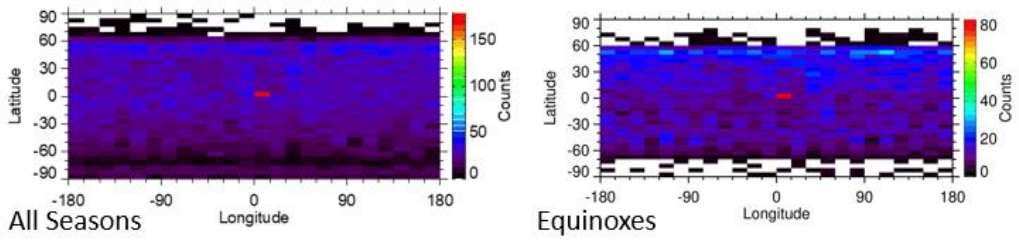

Figure 2.7. Data coverage for all species, altitudes, and solar longitudes shown as a function of latitude and longitude (left) and data coverage excluding Ls periods 60^0 to 150^0 and 240^0 to 330^0 (right). The data counts represent the number of orbits that recorded data in each bin, not the total data available in each bin.

CHAPTER 3

RESULTS AND DISCUSSION

3.1 Results

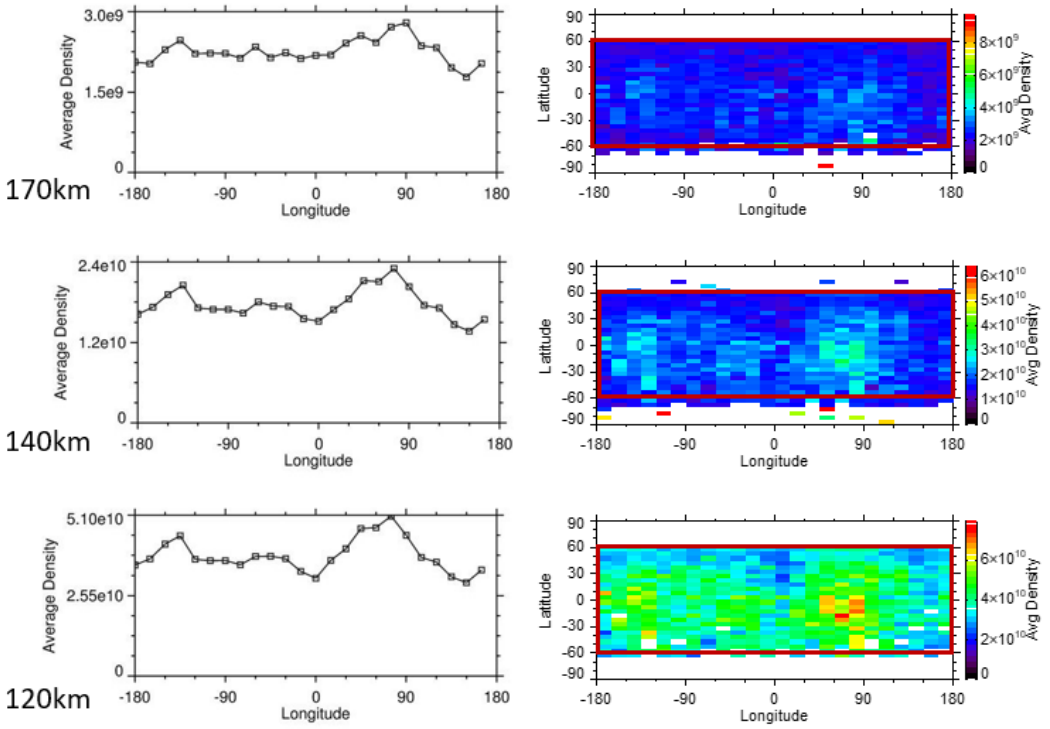

Figure 3.1. CO_2 density variation with longitude during Martian spring and autumn seasons. Densities are plotted on a latitude versus longitude map at 120 km, 140 km, and 170 km (right). The red boxes show the latitude boundaries used to calculate the average density at each longitude (left).

When examining the variation of CO_2 density over all longitudes, two clear density peaks at -135 and 75 degrees occur (Figure 3.1). These

peaks seem to be consistent with the variation that would accompany atmosphere wave 2 structure. It can also be seen that the relative magnitude of the peaks decreases with increasing altitude, which is also expected of the major species undergoing normal atmospheric forcing behavior. In the case of O, however, a different story is presented (Figure 3.2). While the density is still maximized at -135 and 75 degrees, there is

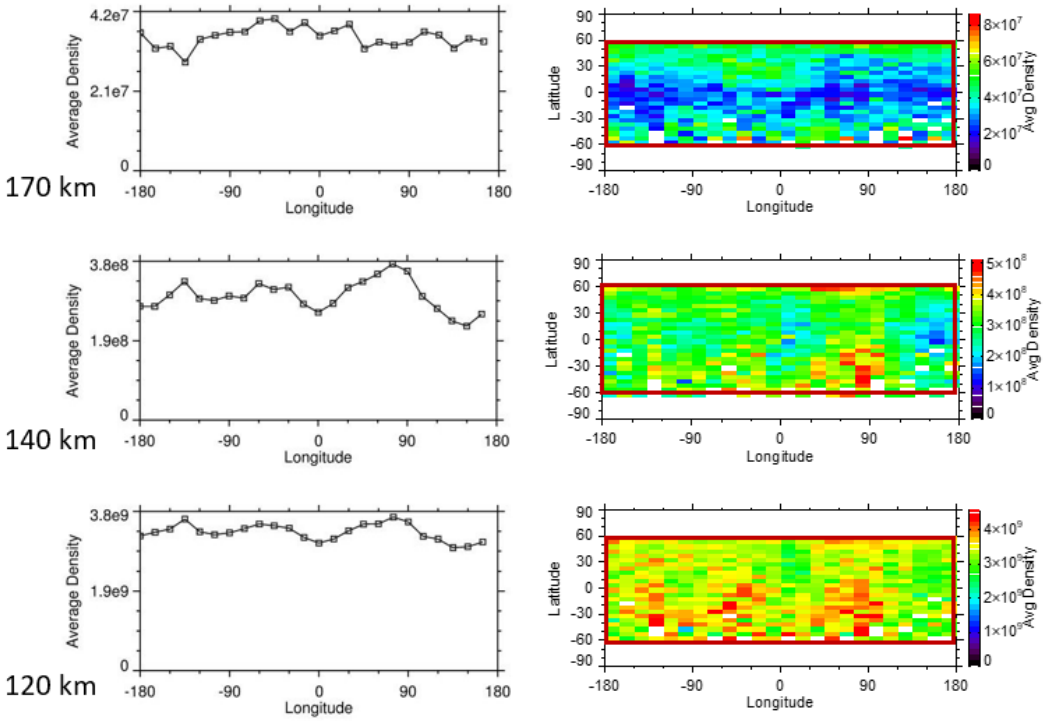

Figure 3.2. O density variation with longitude using data from both equinoxes. Density is plotted in terms of spatial location during Ls from -30^0 to 60^0, and 150^0 to 240^0 (right). Average density at each longitude (left).

now an additional peak present around -60 degrees at the two lower altitudes. At the middle altitude region studied, the percentage difference between the highest and lowest densities is maximized. Additionally, at 170 km for the combined equinox condition, the previous correlation between density and longitude completely shifts and here the only clear peak is at -45 degrees. The level of variation present in the O suggests that the density may be controlled by a mechanism other than atmospheric dynamics, perhaps related to the availability of O_2^+ ions.

Figure 3.3 shows how the CO_2 density varies across latitudes during the combined spring and autumn seasons. The equatorial region generally attains the highest density at all altitudes, which is logical as this is the average subsolar point during the equinox seasons. In comparing the symmetry through the mid-latitudes, the southern hemisphere shows a higher density than the northern hemisphere. This lack of symmetry is the most visible at the lower altitudes and decreases as the altitude increases. There are different structures present when examining the variation of the O density over latitudes (Figure 3.4). At 120 km, there are two peaks; one is in the southern hemisphere at -35 degrees, and the peak with the highest density is at 60 degrees in the northern hemisphere. As the altitude increases, the location of the region with the maximum densities is

inverted from the CO_2 density distribution. The equatorial region becomes a sink, and the mid-latitude regions have the highest density. These differences imply that the mechanisms that control the O density are much more complex than the atmospheric waves that acts as the dominant factor affecting the CO_2 species.

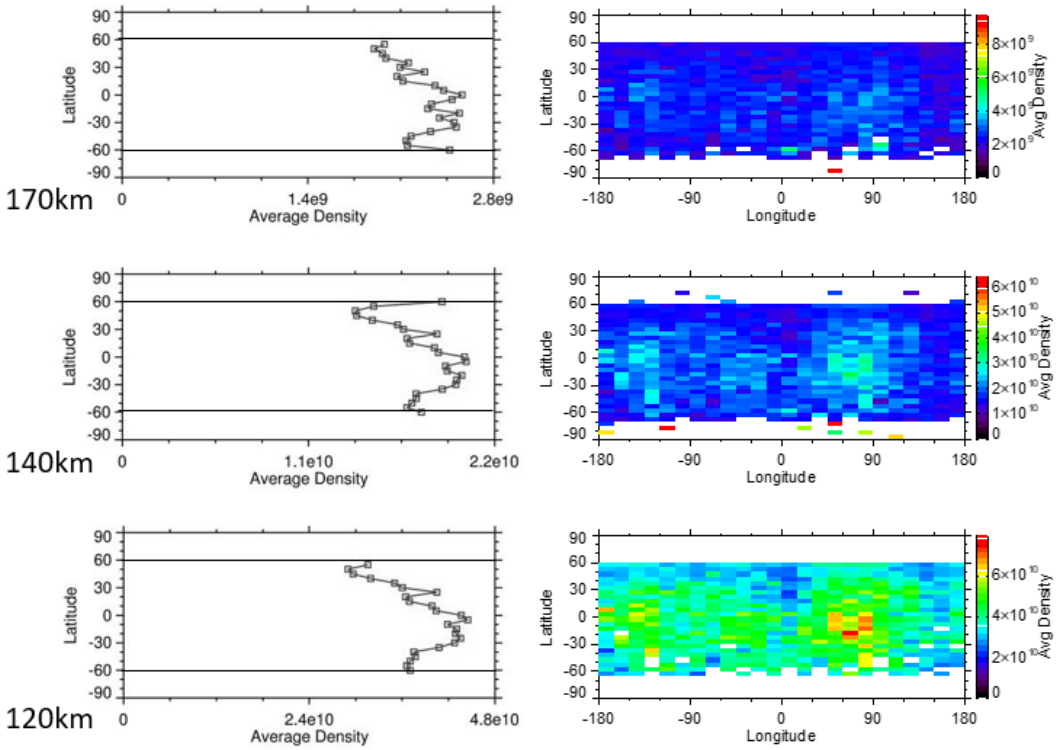

Figure 3.3. CO_2 latitudinal density variation during equinoxes. The right side shows the same CO_2 density maps as in Figure 3.1, but now density is averaged across longitudes to identify a single point at each latitude (left). The lines at 60^0 N and 60^0 S highlight the symmetry (or lack thereof) in the latitudes under examination.

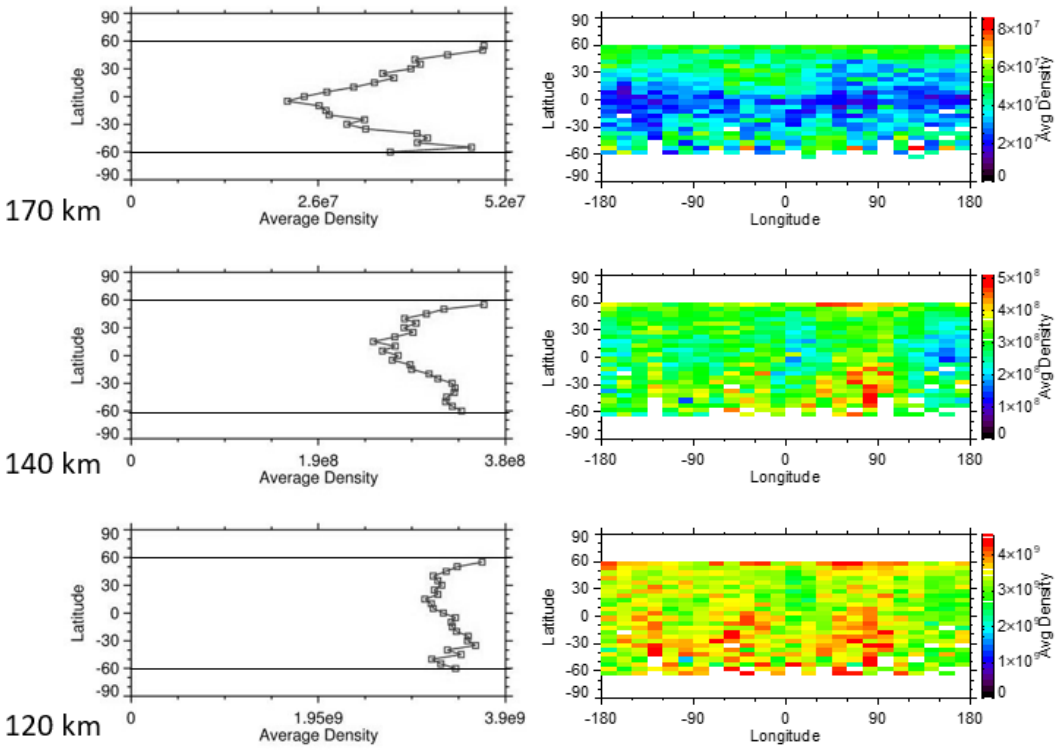

Figure 3.4. Oxygen density variation across latitudes using data from the Martian spring and autumn. Note the presence of a large sink in the equatorial region at 170 km.

Figure 3.5 illustrates the CO_2 density dependence on solar zenith angle. First, it is noticeable in the line plots that the density decreases as the SZA increases, once the SZA is above 50^0. This pattern occurs at all altitudes but becomes the most prevalent at the higher altitudes. Also, these figures show some fluctuation in the density between 0 and 30 degrees, which is also the region where the peak is present. The density

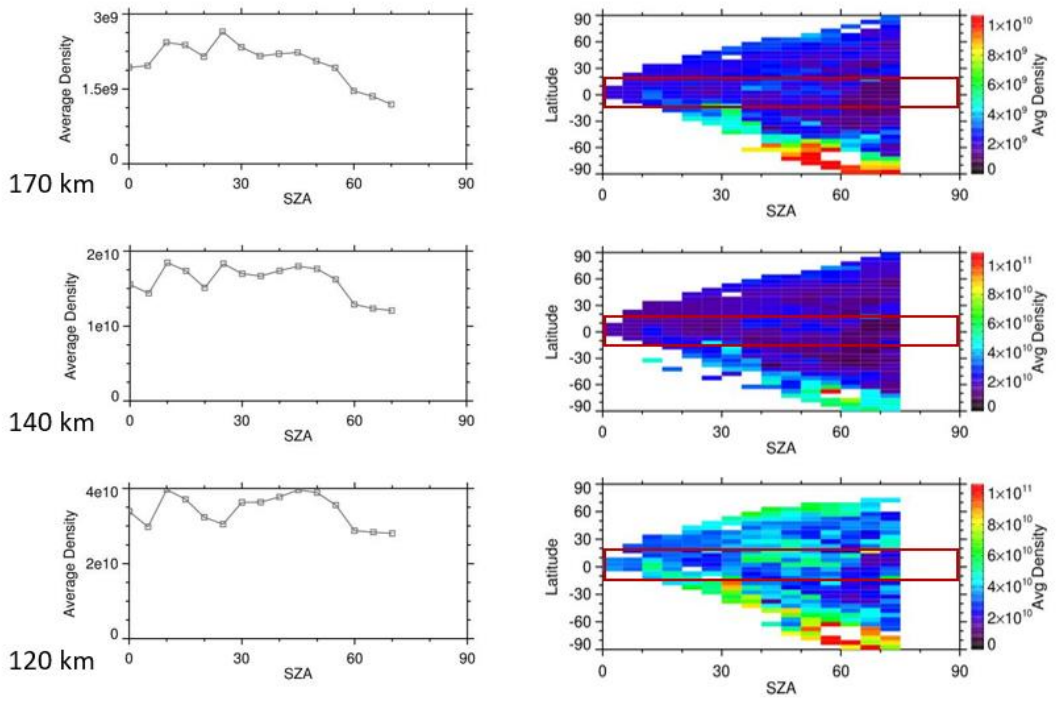

Figure 3.5. Carbon dioxide density dependency on solar zenith angle. The latitude range under examination is 15 degrees S to 15 degrees N to maximize relevant data coverage (right). No data was measured above 75 degrees. CO_2 density begins to decrease above 50 degrees SZA (left).

peaks after the subsolar point at 0 degrees SZA because the atmosphere has inertia and it takes time for the radiation to transfer and cause density enhancement. These results are again concurrent with the factor that CO_2 is primarily driven by solar radiance at higher altitudes, and by turbulence at the lower altitudes near the homopause boundary. However, these structures are not apparent in the oxygen density plots shown in Figure 3.6. At 120 km, the O peak density does occur between 0 and 30 degrees,

but this is a minor peak and there is actually little variation when compared to the other altitudes, which can vary by as much as a factor of 2. Notably at 170 km, the locations with the highest density are at much higher solar zenith angles, between 55 and 70 degrees, further suggesting solar radiation is not the driving factor in O density distributions.

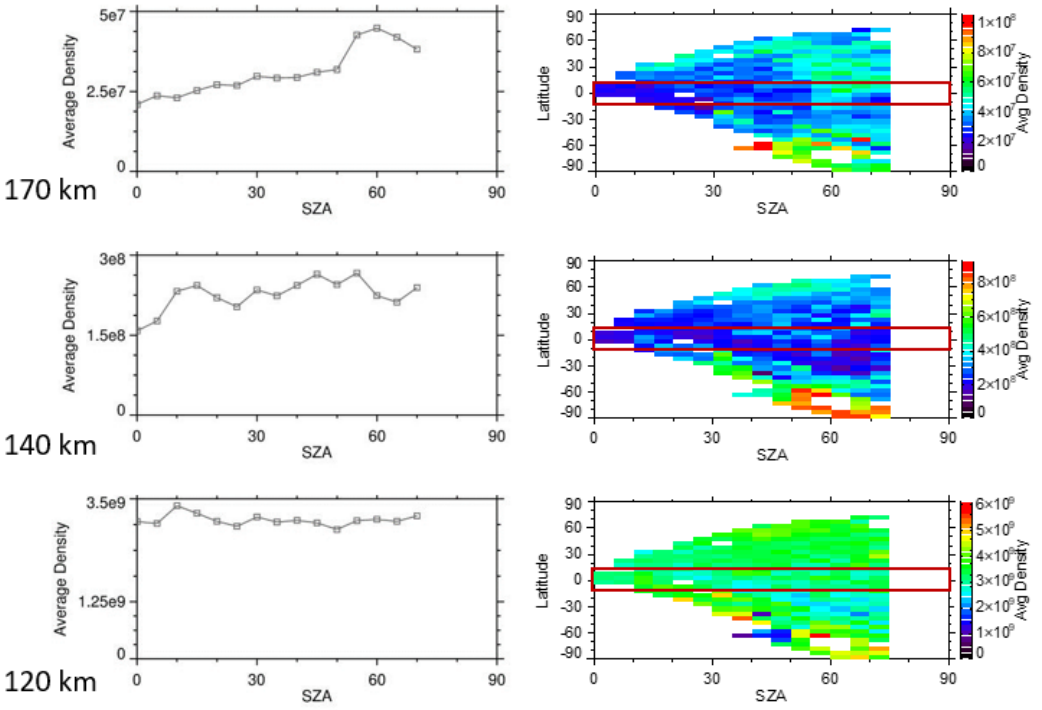

Figure 3.6. Oxygen density dependence on SZA. Each altitude shows an individual structure (left). Data from all seasons was included for SZA plots.

Figure 3.7 shows the CO_2 density distributions as a function of local time, which has density peaks at 14 hours consistently at all altitudes.

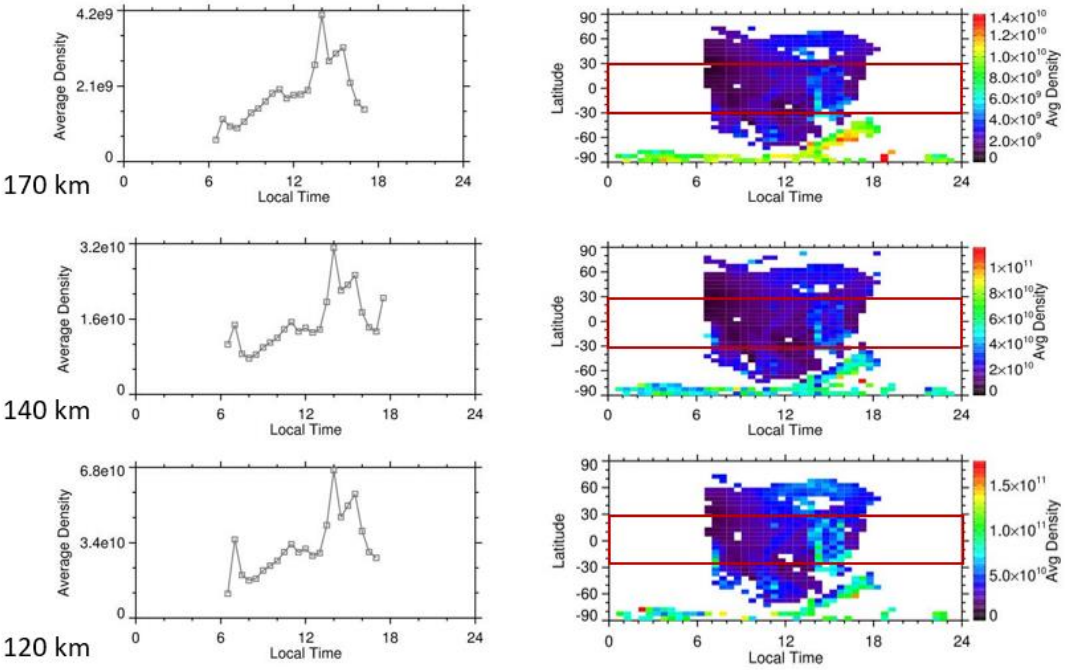

Figure 3.7. The average density of CO_2 at each local time (left). Peaks consistently occur in the afternoon. Density values were taken from 30 degrees N to 30 degrees S, and all seasons are included in the average (right).

Having the density peak during the afternoon is the expected occurrence, due to the solar input increasing thermospheric energy and contributing to the expansion of the atmosphere. Figure 3.8 shows the variation of density of oxygen with local time. At 120 km, the O peaks are less apparent than for CO_2, although the highest density is still occurring at 14 hours. At 140 km, the peak density remains at 14 hours, and is now more than twice the value of the lower densities. The strangest structure occurs at 170 km, where O has dramatic increase in the density during the

morning hours. Oddly enough, this structure persists even when examining the seasonal variation; at this time the cause of it is unknown, although this could be something worthy of further examination.

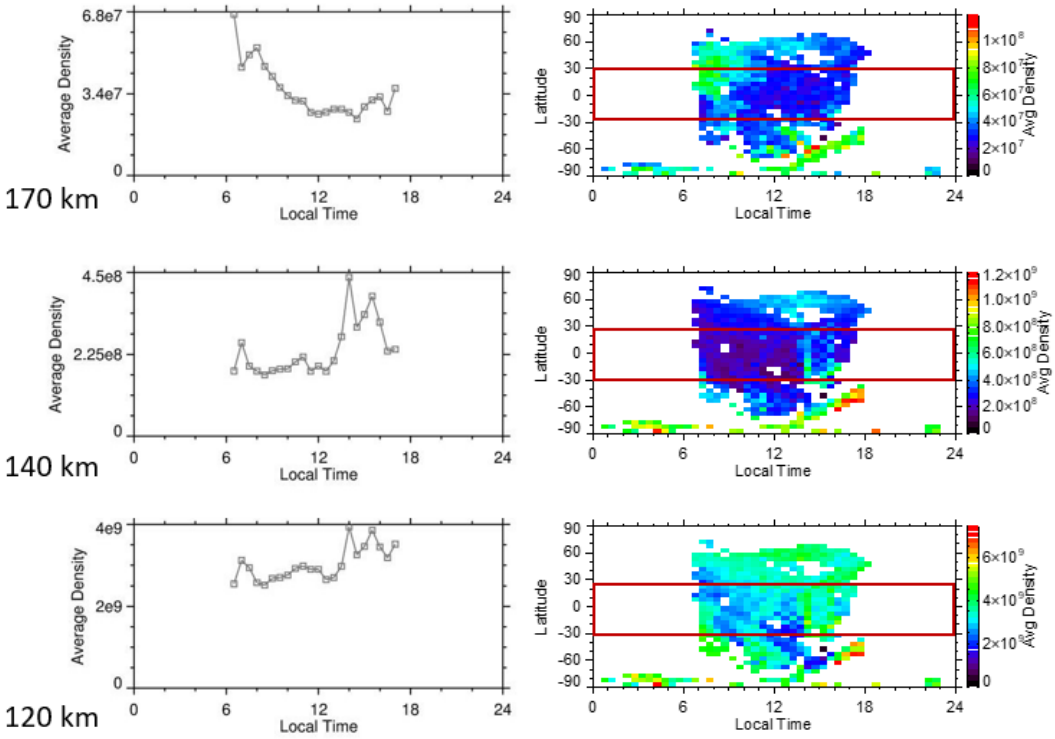

Figure 3.8. Oxygen density dependence on local time. Density peaks in the afternoon at lower altitudes but shifts to a morning peak at 170 km (left).

Across the figures from this study, it can be seen that the CO_2 density is on the order of $1x10^{10}$ cm^{-3} below 150 km and on the order of $1x10^{9}$ cm^{-3} above 150 km, while the O density is initially lower and falls

more rapidly from $1x10^9$ cm^{-3} to $1x10^7$ cm^{-3} across the altitude range from 100 to 200 km. Comparing these results to Lee et al. [2015]'s M-GITM CO_2 and O density distributions at approximately 200 km under solar minimum conditions, it can be seen that the number density of CO_2 was on the same order of magnitude as this study; however, the simulations overestimated the O density by a little over one order of magnitude [10]. Lee et al. [2015] also mentions thermospheric O being strongly affected by global winds, which depend on solar heating and migrating tides [10]; measurements of these variables will also be worth investigating to discover by how much O depends on them. Also comparing results here with the plots of CO_2 and O density as measured by NGIMS as a function of SZA and altitude, we again see similar structures across both studies [12]: CO_2 density decreases as SZA increases above 50 degrees at a set altitude in the thermosphere, and O density is more level across all SZA measured.

3.2 Discussion

The results from the different missions to Mars over the past several decades are constantly increasing human knowledge about the Red Planet and the processes that are ever-present in the atmosphere. As the first mission to solely investigate the atmosphere with the goal of

determining how that atmosphere was primarily lost, MAVEN collects a thorough dataset which includes in situ measurements of neutral species and ions as well as measurements of potential process-driving forces, like solar energetic particles and EUV. It is important to understand the climatology of the upper atmosphere so that the factors controlling atmospheric loss can be better estimated using models developed for this purpose. This data-driven study concludes that the major species on Mars, CO_2, is most affected by solar radiance and atmospheric waves, which are well-described and can easily be accounted for in the models. It is also discovered from this study that O is not as well predicted by these typical processes, and from that we conclude O must follow a more complicated cycle in the Martian upper atmosphere that depends on other influential factors. While this study has postulated some possible variables that could affect the O density distribution, the next step is to investigate the energy input data measured by MAVEN, and determine if any energy sources such as solar EUV, magnetic fields, and ion localization, contribute to the structures presented here in the neutral O density.

CHAPTER 4

CONCLUSIONS AND FUTURE WORKS

This thesis investigated the neutral oxygen and carbon dioxide densities in the Martian thermosphere as measured by the Imaging Ultraviolet Spectrograph (IUVS) instrument on the Mars Atmosphere and Volatile Evolution (MAVEN) mission. Density measurements were processed and plotted in terms of spatial location, and the dependencies on altitude, latitude, longitude, solar zenith angle, and local time were analyzed for both species.

In the thermosphere, the density of the major species, carbon dioxide, is found to behave according to well-documented atmospheric processes such as response to solar radiance and atmospheric waves within the well-mixed lower atmosphere. When examining the variation of CO_2 across the longitude during the equinox (spring and autumn), the presence of an atmosphere wave 2 structure is indicated in the two density peaks present at all altitudes. Also during the equinox seasons, CO_2 density is maximized about the equator, although there is some enhancement in the density in the southern hemisphere through the

midlatitudes. Density variation according to the solar zenith angle shows that CO_2 density decreases as the SZA increases above 50 degrees. It is also seen that the peak density occurs slightly after the subsolar point, which parallels the results drawn from the local time variation. The maximum density occurs at 14 hours which allows time for the radiation to travel through Mars' atmosphere and impact the total density. The study presents a very different set of results for the oxygen density data. Over all the various factors under examination, O shows much more variation in the density structure even just between the three altitude ranges. It is presumed that this is due to the O cycle being more complex than that of CO_2, but this poses the question of what exactly is influencing the distribution of O in the atmosphere.

This was not a fully comprehensive investigation into the effects of these variables on density, but it does provide a stepping-stone from which to start an even more detailed examination. Next steps to expand on the concepts learned in this project include compiling information gathered from MAVEN's other instruments to look into the indirect effects of solar activity on the density distributions in the thermosphere through ion distributions, as well as gathering more data from the IUVS to investigate the seasonal impacts on density more thoroughly. Proceeding a study to determine the sources of the structures presented here in the

neutral oxygen densities, the goal would be to utilize the information learned about the molecular interactions to pursue a study on the hot oxygen escape processes ongoing in the Martian atmosphere today.

REFERENCES

[1] Barabash, S., Fedorov, A., Lundin, R., & Sauvaud, J. A. (2007). Martian atmospheric erosion rates. *Science*, *315*, 501–503. https://doi.org/10.1126/science.1134358

[2] Byrnes, D. V., Longuski, J. M., & Aldrin, B. (1993). Cycler orbit between Earth and Mars. *Journal of Spacecraft and Rockets*, *30*, 334–336. https://doi.org/10.2514/3.25519

[3] Carr, M. H. (1996). *Water on Mars*. Oxford Univ. Press.

[4] Chaffin, M. S., Chaufray, J. Y., Deighan, J., Schneider, N. M., McClintock, W. E., Stewart, A. I. F., et al. (2015). Three-dimensional structure in the Mars H corona revealed by IUVS on MAVEN. *Geophys. Res. Lett.*, *42*, 9001–9008. https://doi.org/10.1002/2015gl065287

[5] Chaufray, J. Y., Deighan, J., Chaffin, M. S., Schneider, N. M., McClintock, W. E., Stewart, A. I. F., et al. (2015). Study of the Martian cold oxygen corona from the O I 130.4 nm by IUVS/MAVEN. *Geophys. Res. Lett.*, *42*, 9031–9039. https://doi.org/10.1002/2015gl065341

[6] Deighan, J., Chaffin, M. S., Chaufray, J.Y., Stewart, A. I. F., Schneider, N. M., Jain, S. K., et al. (2015). MAVEN IUVS observation

of the hot oxygen corona at Mars. *Geophys. Res. Lett.*, *42*, 9009–9014. https://doi.org/10.1002/2015gl065487

[7] Frey, W. R., Lin, C. S., Garvin, M. B., & Acebal, A. O. (2014). Modeling the thermosphere as a driven-dissipative thermodynamic system. *Space Weather*, *12*, 132–142. https://doi.org/10.1002/2013sw001014

[8] Jakosky, B. M., Lin, R. P., Grebowsky, J. M., Luhmann, J. G., Mitchell, D. F., Beutelschies, G., et al. (2015). The Mars Atmosphere and Volatile Evolution (MAVEN) Mission. *Space Sci. Rev.*, *195*, 3–48. https://doi.org/10.1007/s11214-015-0139-x

[9] Jakosky, B. M., & Haberle, R. M. (1992). The seasonal behavior of water on Mars, in *Mars*, edited by H. Kieffer et al., pp. 969–1016, Univ. of Ariz., Tucson.

[10] Lee, Y., Combi, M. R., Tenishev, V., Bougher, S. W., & Lillis, R. J. (2015). Hot oxygen corona at Mars and the photochemical escape of oxygen: Improved description of the thermosphere, ionosphere, and exosphere. *J. Geophys. Res. Planets*, *120*, 1880–1892. https://doi.org/10.1002/2015je004890

[11] Mahaffy, P. R., Webster, C. R., Atreya, S. K., Franz, H., Wong, M., Conrad, P. G., et al. (2013). Abundance and isotopic composition of

gases in the Martian atmosphere from the Curiosity rover, *Science, 341*, 263-266. doi:10.1126/science.1237966

[12] Mahaffy, P. R., Benna, M., Elrod, M., Yelle, R. V., Bougher, S. W., Stone, S. W., & Jakosky, B. M. (2015). Structure and composition of the neutral upper atmosphere of Mars from the MAVEN NGIMS investigation. *Geophys. Res. Lett.*, *42*, 8951–8957. https://doi.org/10.1002/2015gl065329

[13] Mars Exploration Program and the Jet Propulsion Laboratory for NASA's Science Mission Directorate. (2014). *NASA's Mars Exploration Program*. https://mars.nasa.gov/

[14] Mayyasi, M., Clarke, J., Bhattacharyya, D., Deighan, J., Jain, S., Chaffin, M., et al. (2017). The variability of atmospheric deuterium brightness at Mars: Evidence for seasonal dependence. *J. Geophys. Res. Space Phys.*, *122*. https://doi.org/10.1002/2017ja024666

[15] McClintock, W. E., Schneider, N. M., Holsclaw, G. M., Clarke, J. T., Hoskins, A. C., Stewart, I., et al. (2014). The Imaging Ultraviolet Spectrograph (IUVS) for the MAVEN Mission. *Space Sci. Rev.*, *195*, 75–124. https://doi.org/10.1007/s11214-014-0098-7

[16] Medvedev, A. S., Nakagawa, H., Mockel, C., Yiğit, E., Kuroda, T., Hartogh, P., et al. (2016). Comparison of the Martian thermospheric density and temperature from IUVS/MAVEN data and general

circulation modeling. *Geophys. Res. Lett.*, *43*, 3095–3104. https://doi.org/10.1002/2016gl068388

[17] Nier, A. O., & Mcelroy, M. B. (1977). Composition and structure of Mars' Upper atmosphere: Results from the neutral mass spectrometers on Viking 1 and 2. *J. Geophys. Res., 82*, 4341–4349. https://doi.org/10.1029/js082i028p04341

[18] Ryden, B., & Peterson, B. M. (2010). *Foundations of Astrophysics*. Addison-Wesley.

BIOGRAPHICAL INFORMATION

Emily Ann Curtis earned her first Bachelor of Science degree in Biology from the University of Texas at Arlington in 2015, and while in pursuit of that degree discovered an interest in the applications of physics. She stayed at the University of Texas at Arlington to complete a second Bachelor of Science degree in Physics in 2018, when she graduated summa cum laude. As an undergraduate, she started doing research in space physics under the guidance of Dr. Yue Deng. She ultimately continued that research in graduate school and earned the Master of Science in Physics in 2020 from the University of Texas at Arlington.